BIO-INSPIRED DESIGN OF BIPOLAR PLATE FLOW FIELDS FOR POLYMER ELECTROLYTE MEMBRANE FUEL CELLS

Nannan Guo[1], Ming C. Leu[1], and Maoliang Wu[2]

[1]Department of Mechanical and Aerospace Engineering, Missouri University of Science and Technology, Rolla, MO 65409, USA
[2]Shanghai University of Electric Power, Shanghai, 200090, China

REVIEWED, August 17 2011

Abstract

The flow field of a bipolar plate distributes hydrogen and oxygen for polymer electrolyte membrane (PEM) fuel cells and removes the produced water from the fuel cells. It greatly influences the performance of fuel cells, especially regarding reduction of mass transport loss. Flow fields with good gas distribution and water removal capabilities reduce the mass transport loss, thus allowing higher power density. Inspired by natural structures such as veins in tree leaves and blood vessels in lungs, which efficiently feed nutrition from one central source to large areas and are capable of removing undesirable by-products, a mathematic model has been developed to optimize the flow field with minimal pressure drop, lowest energy dissipation, and uniform gas distribution. The model can be used to perform optimal flow field designs, leading to better fuel cell performance for different sizes and shapes of bipolar plates. Finite element modeling (FEM) based simulations and in-situ experiments were conducted to verify some of the flow field designs obtained using the developed mathematic model.

1. Introduction

Polymer electrolyte membrane (PEM) fuel cells have great advantages as an energy conversion device such as low-temperature operation, high-power density, fast start-up, system robustness, and low emissions. They are very promising alternative power sources for automotive applications [1]. The flow field of a bipolar plate supplies fuel and oxygen to reaction sites and removes reaction products (i.e., liquid water) out of the fuel cell, significantly effecting the performance of PEM fuel cells. Previous studies have demonstrated that the power density of a fuel cell can increase by 20-30% with a proper flow field design [2, 3].

Numerous flow field designs have been proposed and investigated. These designs can be classified into four categories of layouts: pin-type, parallel, serpentine and interdigitated [4]. Among them parallel and serpentine designs are the most widely known and utilized. Parallel designs usually provide low pressure drop, and serpentine designs usually give high fuel cell performance. However, lots of drawbacks are associated with these two kinds of designs. Parallel flow fields have multiple flow paths. Because gases flow preferentially through the least resistant channels, stagnant areas tend to form at various areas of parallel channels, lowering the transport efficiency of the reactants. Serpentine flow fields [5] typically result in a relatively long reactant flow path, leading to a substantial pressure drop. Consequently, significant parasitic power loss is associated with the fuel supply (as high as over 35% of the stack's output power), especially when the stack contains a large number of cells or when fuel cells with large active areas are

used. Additionally, reactant concentration significantly decreases from the inlet to the outlet of the flow channel. This decrease leads to considerable Nernst losses and non-uniform current density distribution, reducing both the performance and the lifetime of PEM fuel cells [6].

Besides conventional flow field layouts, researchers have begun to investigate flow field designs with inspirations from nature [7-12]. These bio-inspired flow field designs have demonstrated advantages in distributing reactants and enhancing performance. Kloess et al. [7] combined serpentine and interdigitated patterns with a leaf/lung layout to design a bio-inspired flow layout. They reported that these new designs improved pressure distribution, decreased pressure loss, and increased power density as compared to pure serpentine and interdigitated designs. Chapman et al. [8, 9] claimed that their bio-mimetic designs enhanced the performance of PEM fuel cells by 16%. They stated that their designs comprised main and sub-feed channels and that tapered, non-linear channels could improve performance. The above studies have shown the potential benefits of incorporating natural structures into flow field designs. However, the bio-inspired designs that have been investigated thus far are only bio-mimetic, i.e. they mimic some particular structures in nature's biological systems. There is a lack of comprehensive and systematic studies on how to create an optimal bio-inspired design of flow fields for bipolar plates.

Very recently, some researchers have developed optimization models to optimize flow field designs in order to improve the performance of PEM fuel cells. Wang et al. [13] integrated a conjugated-gradient scheme and a three-dimensional fuel cell numerical model to optimize the depth of tapered flow channels for serpentine designs, which enhances the oxygen transport rate and local current density. Peng et al. [14] proposed an analytical model to optimize the depth of flow channels in a slotted-interdigitated flow field in order to obtain an even flow distribution in the channels. However, all these optimization models were developed based on a certain flow layout (serpentine or interdigitated). Moreover, only the channel's width or depth is optimized to achieve the expected flow properties, which limits the optimization space of flow field designs.

With inspiration from the idea that nature structures (e.g., leaf veins) provide excellent mass transport with uniform pressure distribution and low energy dissipation, the present study presents an optimization model to generate flow field designs with these properties. The generated designs include designs of flow field layouts and channel geometries. The model starts with small grids on the flow fields and generates optimum designs with structures similar to nature. This is intended to lead to minimum pressure drop, uniform pressure distribution, and better fuel cell performance. Given the flow field shapes and the locations of the inlet and outlet, one example of the generated designs based on the optimization model has been investigated with FEM simulation and compared with the conventional parallel and serpentine designs. The results show that the proposed design provides better fuel cell performance, with more uniform pressure distribution and less pressure drop over the flow field.

2. Mathematical Algorithm

2.1 Flow field

The flow field design involves the layout of the flow field and channel cross-section geometries including shape and dimensions. Usually for the flow field design, researchers start

from a particular flow field layout (e.g., serpentine [13] or interdigitated [14]) and then optimize the shape or dimensions (e.g., width and depth) to achieve desired results. Our approach starts from the flow field grids (see Fig. 1), where the flow field is meshed by $N \times N$ nodes and $(2 \times N \times N + 2 \times (N - 1))$ channels with pre-set dimensions. After optimizing the channel dimensions, the corresponding flow field layout is determined because the flow field layout essentially is the configuration of all the flow channels.

2.2 Optimization model

The mathematic model is formatted to a constrained optimization problem. The steps for solving the problem are as follows: (1) Mesh the flow field into small grids, which can be triangle, rectangular, or hexagonal; (2) Establish flow relationships using these grids, and define the objective function and constraints; (3) Optimize the objective function using the Lagrangian method; and (4) Generate the optimum flow field design. The flow chart of the optimization model is given in Fig. 1.

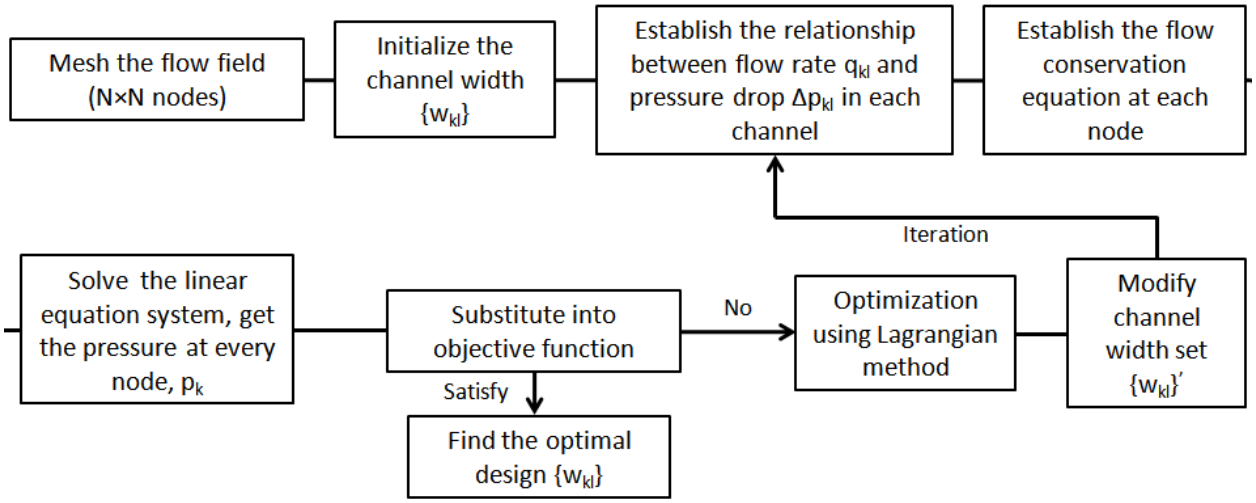

Fig. 1 Flow chart of the optimization model.

2.2.1 Flow relationship

In the proposed optimization model, several assumptions are made. Firstly, the flow through the channels is laminar flow. This assumption is fairly true in reality, since, under most conditions, gas flow in fuel cell channels is laminar; only at extremely high flow rates can gas flow become turbulent [15]. Secondly, only the pressure drop along each channel is considered in the model, while the pressure losses at the junctions of channels, which could be caused by abrupt changes in flow direction or channel dimension, are ignored. Thirdly, the fluid in the flow channel obeys ideal gas laws. Finally, the overlap area of channels at the junctions is neglected (which implies that the calculated total channel area is greater than the actual total channel area).

For laminar flow, the pressure drop in a channel for a given flow rate can be determined by:

$$\Delta p = f \frac{L}{D_h} \frac{\rho v^2}{2} \tag{1}$$

where L is the channel length, ρ is the fluid density, v is the average flow velocity in the channel, D_h is the hydraulic diameter, and f is the friction factor. For a channel with a rectangular cross-section shape (width: w, depth: d) [15],

$$D_h = \frac{4A_c}{P} = \frac{2wd}{w+d} \tag{2}$$

where A_c and P are the channel's cross-section area and perimeter, respectively. For laminar flow,

$$f = \frac{64}{Re} \tag{3}$$

where Re is the Reynolds Number of the flow,

$$Re = \frac{\rho v D_h}{\mu} \tag{4}$$

where μ is the fluid viscosity. The volumetric flow rate has the relationship

$$q = v * A_c = \frac{\pi {D_h}^2 v}{4} \tag{5}$$

By substituting equations (3-5) into equation (1), the pressure drop in a channel can be expressed in terms of flow rate and the channel's dimensions as

$$\Delta p = \frac{128\mu L q}{\pi {D_h}^4} \tag{6}$$

Consider a flow field composed of N×N nodes that are connected by channels (Fig. 2). Channel (k, l) is designated as the channel connecting two neighboring nodes k and l. Therefore, the pressure drop in each channel (k, l) can be determined once the flow rate and the channel dimensions are known:

$$\Delta p_{kl} = \frac{128\mu L_{kl} q_{kl}}{\pi {D_{kl}^h}^4} \tag{7}$$

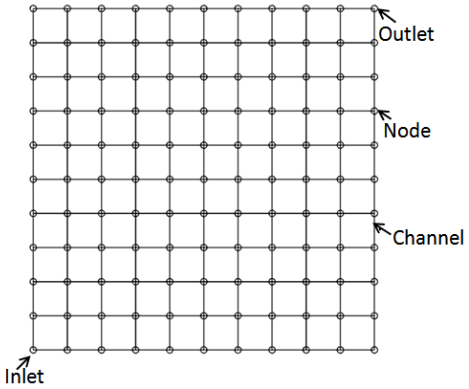

Fig. 2 Mesh of the flow field with N×N nodes (one inlet, one outlet), which were connected by $(2\times N\times N+2\times(N\text{-}1))$ channels.

There are varying volumetric flow rates through the channels. For a given node k, the flow-in rate should equal the flow-out rate. The relationship can be expressed as a zero sum of all the flow rates through a node if the flow-in rate is defined as positive and the flow-out rate is negative, i.e.

$$\sum_k q_{kl} = 0 \tag{8}$$

2.2.2 Constraints

The wider the channel is, the lower the pressure drop that occurs in the channel. However, the channel cannot be arbitrarily wide. The total surface area of the channel is

$$S_c = \sum_{(k,l)} L_{kl} w_{kl} \tag{9}$$

This area must be less than the area of the flow field. Surface area is an important parameter in the design of a bipolar plate flow field because it directly influences the mass transport efficiency and the electrical conductivity of bipolar plates. Because the total flow field area equals the sum of the surface area of channels and the land area, which is the contacting area between bipolar plates and the gas diffusion layer (GDL), a larger surface area of channels would be good for mass transport but would reduce the conduction of electricity and eventually the fuel cell's performance. Therefore, a trade-off between mass transport and electrical conductivity is needed in order to decide a proper channel surface area. In the present work, assuming that the surface area is constant, and taking 75% of the total flow field area as an example. Then,

$$S_c = \frac{3}{4} A \tag{10}$$

where A is the flow field area of the fuel cell.

2.2.3 Objective function

One important concept in PEM fuel cell design is the limiting current density, j_L, which is the current density when the reactant concentration decreases to zero at the surface of the catalyst layer. In other words, j_L is the highest current density that the fuel cell can operate at under a certain condition. According to the electrochemical reaction and diffusion law, the limiting current density of a fuel cell [15] is:

$$j_L = nFD^{eff} \frac{c^0}{\delta} \tag{11}$$

where n is the number of moles of electrons transferred for one mole of reactant, e.g. for O_2, $n = 4$, F is Faraday's constant, D^{eff} is the effective diffusivity within the GDL, c^0 is the reactant concentration in the channel, and δ is the thickness of the GDL. In order to improve the performance of a fuel cell, we need to increase the limiting current density [15] and thus the reactant concentration c^0 in the flow channel by optimizing the flow field design. Note that the reactant concentration decreases along the flow channel due to the reaction consumption and pressure drop from the inlet to the outlet. If the cathode is considered, the concentration of oxygen in the flow channel (assuming air is used) is:

$$c_{O_2}^0 = 0.21 \frac{N}{V_c} = 0.21 \frac{P}{RT} \tag{12}$$

where N is the amount of gas in moles, V_c is total the volume of channels, P is the pressure in channels, R is the ideal gas constant, and T is the absolute temperature. From equation (12), maintaining a high reactant concentration means maintaining a high and uniform pressure over the flow field, which in turn requires obtaining the lowest pressure drop over the flow field (if the same inlet pressure is used). Thus, the objective function is:

$$Minimize\ F = \sum_{(k,l)} \Delta p_{kl} = \sum_{(k,l)} \frac{128 \mu L_{kl} q_{kl}}{\pi D_{kl}^{h\ 4}} \tag{13}$$

2.2.4 Optimization algorithm

The pressure drop in one channel can be determined by equation (7). To simplify the analysis, flow resistance r_{kl} is defined as:

$$r_{kl} = \frac{128\mu L_{kl}}{\pi D_{kl}^{h\,4}} \tag{14}$$

Note that r_{kl} is only related to the channel geometry (because μ is a constant for a given gas). Equation (7) can be simplified:

$$\Delta p_{kl} = r_{kl} q_{kl} \tag{15}$$

According to equation (8), the equation can be established for every node k:

$$\sum_k q_{kl} = \sum_k \frac{\Delta p_{kl}}{r_{kl}} = \sum_k \frac{P_l - P_k}{r_{kl}} = 0 \tag{16}$$

where P_l and P_k are the pressures at nodes k and l, respectively.

Based on the above discussion, the design of the flow field of a bipolar plate is converted to an optimization problem with the objective function in equation (13) subjected to the constraint in equation (10). The known and unknown parameters are shown in Tables 1 and 2, respectively. In this model, both channel width $\{w_{kl}\}$ and depth $\{d_{kl}\}$ can be treated as variables; however, for ease of design, only one of them is chosen as a variable, while the other is kept constant [13]. Channel width $\{w_{kl}\}$ is chosen as a variable in our study, and a depth of 1.5 mm is used for all channels because channel width has a greater influence on the contact area of the reactant, the GDL and, consequently, the mass transport. The flow properties within channels with the same hydraulic diameter are almost the same; therefore, according to equation (6), channels with square cross-sections are used in the model first to simplify the calculation, where hydraulic diameter equals channel width from equation (2). Once the optimized hydraulic diameter $\{D_{kl}^h\}$ is determined from the optimization model, the rectangular channel width can be calculated from equation (2).

Table 1 Known parameters in the optimization model.

Number of nodes	Total flow rate	Active area	Total channel area	Channel length	Channel depth	Fluid viscosity	Location of inlet and outlet
$N \times N$	Q	A	S_c	$\{L_{kl}\}$	$\{d_{kl}\}$	μ	Inlet: bottom left corner; Outlet: top right corner/uniform sinks.
N=11 N=16	4.3×10^{-5} m^3/s	5×5 cm^2	0.75A	$\frac{5}{N-1}$ cm	1.5 mm	1.79×10^{-5} kg/m s*	

*The dynamic viscosity of air at 298 K.

Table 2 Unknown parameters in the optimization model.

Channel width	Pressure drop along channel	Flow rate in channel
$\{w_{kl}\}$	$\{\Delta p_{kl}\}$	$\{q_{kl}\}$

Next, the Lagrangian method [16-19] is used to solve the constrained optimization problem. The Lagrangian function is defined as

$$\phi\left(\{q_{kl}\}, \{D_{kl}^h\}\right) = \sum_{(k,l)} \frac{128\mu L_{kl} q_{kl}}{\pi D_{kl}^{h\,4}} - \lambda \sum_{(k,l)} L_{kl} D_{kl}^h \tag{17}$$

where λ is the Lagrange multiplier. The necessary conditions for a minimum F subjected to constraint (10) are

$$\frac{\partial \phi}{\partial q_{kl}} = 0, \quad \frac{\partial \phi}{\partial D_{kl}^h} = 0 \tag{18}$$

Consider the derivative of ϕ with respect to D_{kl}^h

$$D_{kl}^h = \left(-\frac{512\mu q_{kl}}{\lambda \pi}\right)^{\frac{1}{5}} \tag{19}$$

Then, with the constraint (10), in the minimum configuration the scaling relationship between hydraulic diameter and flow rate is

$$D_{kl}^h = \frac{q_{kl}^{\frac{1}{5}}}{\sum_{(m,n)} q_{mn}^{\frac{1}{5}} L_{mn}} C \tag{20}$$

where the constant $C = \frac{3}{4}A$.

To start the calculation, a set of values (e.g., 1.5 mm for all channels) is used to initialize the hydraulic diameter $\{D_{kl}^h\}$. Then, the flow resistance for each channel can be determined from equation (14), the pressure value at each node ($N \times N$ unknowns) can be calculated by solving these $N \times N$ equations (16), and then the total pressure drop and the flow rate in each channel can be obtained from equations (13) and (15), respectively. The iteration process continues; at each iteration, the hydraulic diameter varies according to the scaling relationship given in equation (20), until the minimum pressure drop is achieved, thereby resulting in the optimum flow field design. A Matlab program was developed to implement this optimization algorithm.

2.3 Optimized flow field designs

Several optimal designs for different situations (i.e., positions of inlets and outlets) were obtained for a 5×5 cm^2 flow field, with the total surface area of channels being 75% of the total flow field area. The parameters, including the total flow rate, are given in Table 1 for known parameters and in Table 2 for unknown parameters. The results for several scenarios are shown in Fig. 3. For all scenarios, the inlet is located at the bottom left corner. Fig. 3(a) shows the initial mesh of the square flow field with 11×11 nodes and a pre-set channel width. Fig. 3(b) depicts an optimum result obtained from the proposed model; the pressure drop in the flow field is 24.3 Pa, and the outlet is located at the top right corner. In Fig. 3(c), the single outlet was changed to uniform sinks over all the nodes. If the inlet flow rate is Q, then the flow rate of $\frac{Q}{N \times N - 1}$ would leave each channel to go into the GDL for reaction. In this optimum situation, all the reactant is consumed, and, moreover, the reactant is distributed uniformly to the GDL. Note that, realistically, the diffusion of reactant from the flow channel to the GDL occurs along the channels. Here, we count only the total amount along one channel at the corresponding nodes. The optimized design of this situation is shown in Fig. 3(c), and the calculated pressure drop is 9.42 Pa. Along with the flow field designs including loops like those in Fig. 3(b) and (c), the designs without loops have also been investigated. Fig. 3(d) shows the design with 11×11 nodes on the flow field, and the pressure drop calculated is 6.02 Pa. Fig. 3(e) shows the design obtained from the flow field with 16×16 nodes, and the pressure drop calculated is 20.17 Pa. Both of these designs are based on a uniform-sink outlet. The above design examples show the capabilities of this basic mathematic algorithm, which obtains the desired flow field design with the desired

properties from well-defined objective functions and constraints. It can be used for flow fields of any shape and inlets and outlets at any locations. CAD models also were built based on the channel width data generated from the optimization model for FEM analysis and fabrication of bipolar plates with flow channels designed for experimental evaluation. Although the optimized designs have complex geometries with tapered channels, they can be fabricated easily with the Selective Laser Sintering (SLS) process [20, 21]. Fig. 4 shows the corresponding CAD models from Fig. 3(c) and (d).

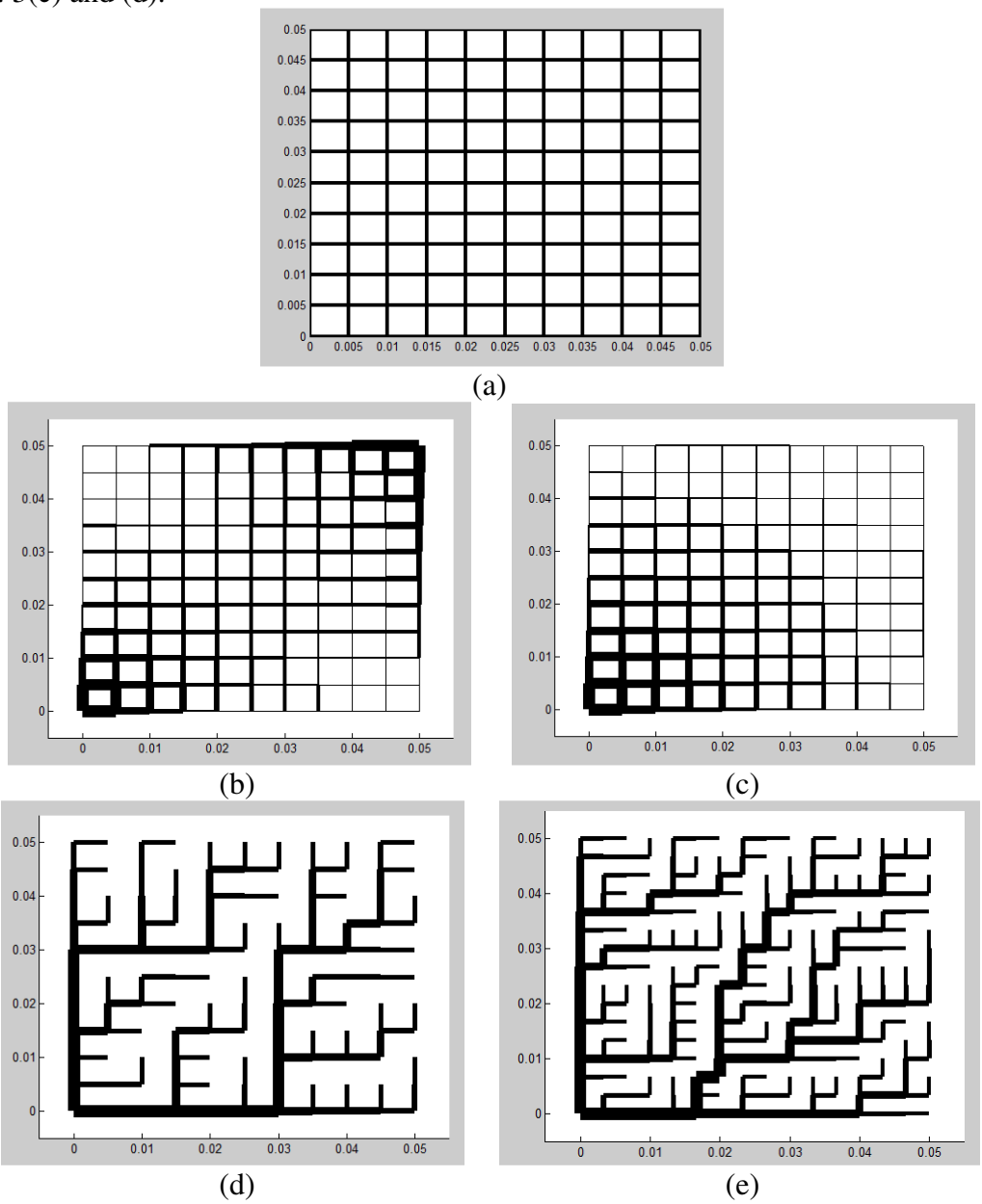

Fig. 3 (a) Initial mesh of the flow field (unit: m); Optimum flow field designs obtained from the optimization model when (b) N = 11, one inlet with one sink; (c) N = 11, one inlet with uniform sink; (d) flow field without loops, N = 11, one inlet with uniform sinks; (e) flow field without loops, N = 16, one inlet with uniform sinks. (In the figure, the width of lines indicates the width of flow channels, but the actual flow field designs may not look as they appear in the Matlab figures because the channel width ratios may be different from the line width ratios).

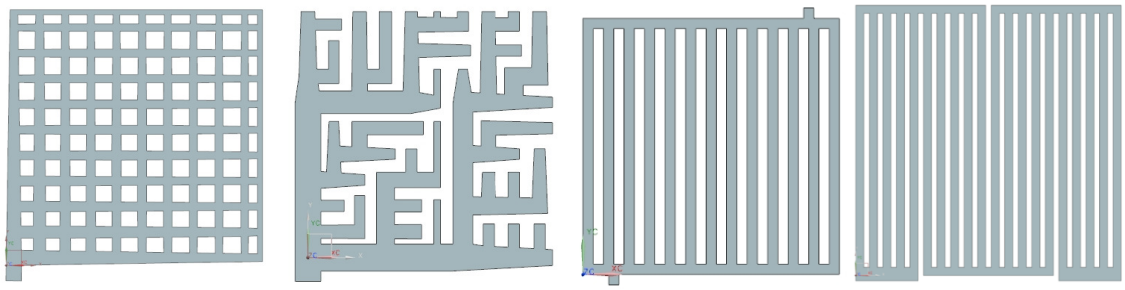

(a) (b) (c) (d)

Fig. 4 CAD models for the optimized designs in (a) Fig. 3(c) design, (b) Fig. 3(d) design, (c) parallel design, and (d) multiple-serpentine design.

3. FEM Simulation

The operation of PEM fuel cells involves complicated processes including electrochemical reaction, multi-flow, and thermal mechanics. Most of these processes are difficult or even impossible to investigate with experimental study only. Finite element modeling (FEM) can be used to provide predictive models of PEM fuel cell operation [23, 24]. In our present work, an FEM model of a PEM fuel cell was developed with the commercial software FLUENT and used to investigate the performance of a fuel cell, including polarization curves, pressure distribution, and current density distribution within the fuel cell for a parallel design, a serpentine design, and an optimized flow field.

To verify that the FEM model established was correct and sufficiently accurate, the results from our FEM simulation were compared with the experimental results from reference [22], as shown in Fig. 5. The flow field was 5×4.92 cm^2 with a serpentine design, the channel width and depth were 1.2 mm and 1 mm, respectively, and land width was 1.2 mm. The operation conditions were listed in Table 3. The parameters used in the FEM models were given in Table 4. Fig. 5 shows that the FEM simulation results could closely predict the actual performance of PEM fuel cells, although the voltage and power density predicted by the FEM simulation were slightly higher than the experimental results due to neglecting some losses.

Table 3 The operation conditions for comparing the FEM simulation with experimental results.

Operation temperature (K)	323
Operation pressure (atm)	1
H_2 flow rate (kg/s)	6.98×10^{-7}
O_2 flow rate (kg/s)	1.13×10^{-5}
Humidity	100%

Table 4 Parameters used in the FEM simulation study.

Reference current density at anode (A/cm^2)	9.48×10^{5}
Reference current density at cathode (A/cm^2)	1.0×10^{4}
GDL and catalyst layer porosity	0.4
GDL and catalyst layer permeability (m^{-2})	5.68×10^{10}
Exchange coefficient at anode	0.5
Exchange coefficient at cathode	1.5
Concentration exponent at anode	0.5
Concentration exponent at cathode	1.0

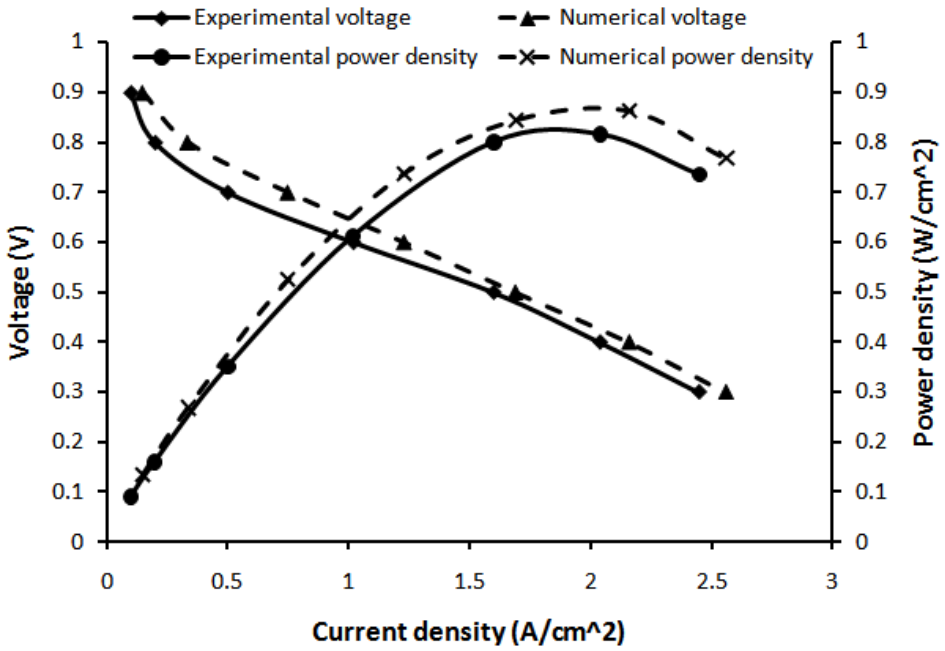

Fig. 5 Comparison of polarization curves and power density obtained from our FEM simulation and experimental results from [22].

The FEM model was used to compare numerically the performance of the parallel (Fig. 4(c)), multiple-serpentine (Fig. 4(d)), and optimum designs (Fig. 4(a)) under the operation conditions given in Table 5. Fig. 6 shows the polarization curves and power density curves for the three different designs. Fig. 7 shows the pressure distribution in the flow channels on the cathode side and also the pressure distribution at the interface of the GDL and catalyst layer, where the operation voltage is 0.55 V. The corresponding oxygen distribution and current density distribution at the interface of the GDL and catalyst layer are shown in Figs. 8 and 9, respectively.

Table 5 Operation conditions used in the FEM simulation for different flow field designs.

Operation temperature (K)	353
Operation pressure (atm)	2.0
H_2 flow rate (kg/s)	2.0×10^{-6}
Air flow rate (kg/s)	5.2×10^{-5}
Humidity	100%

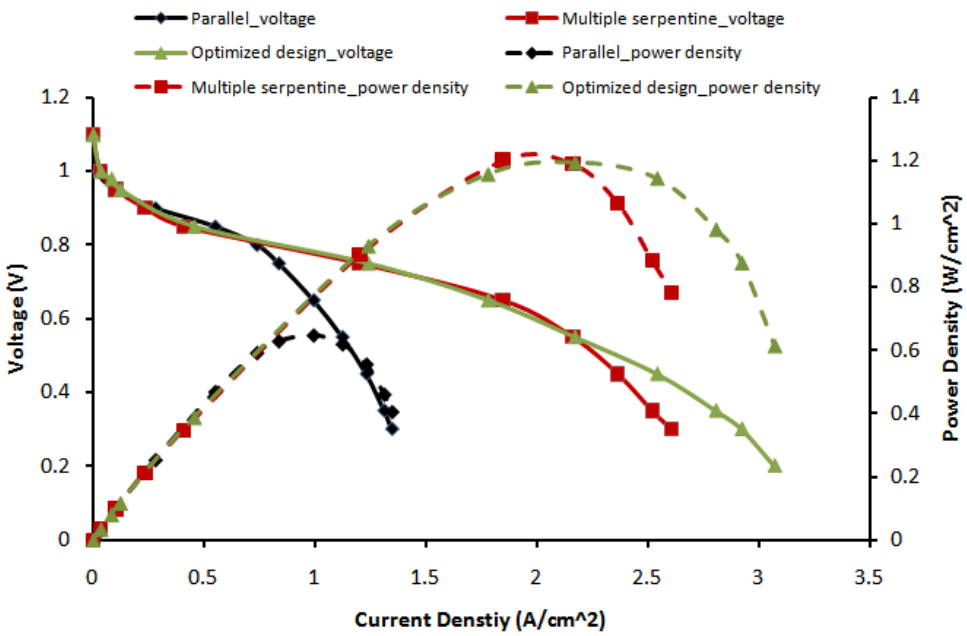

Fig. 6 Polarization curves and power density curves for the parallel design, the multiple-serpentine design, and the optimized design.

Table 6 Pressure drop from inlet to outlet for different flow field designs (cathode side).

Designs	Parallel design	Multiple-serpentine design	Optimized design
Pressure drop (Pa)	226	1011	270

4. Discussion

Fig. 6 clearly shows that the parallel design has the worst performance. This is expected because stagnant areas tend to form in the parallel channels, resulting in poor mass transport capabilities [4]. This point is supported by the distribution of pressure and oxygen (Figs. 7 and 8). In some channels of the parallel flow field (e.g., channels 4 through 8 from left to right, Fig. 7(a, b)), the pressure difference is very small; therefore, no reactant is flowing through these channels and stagnant areas form. As shown in Fig. 8(a), no oxygen is supplied in these areas. The multiple-serpentine design performs similarly to the optimized design obtained from the proposed optimization model, when the fuel cells work below 2.2 A/cm^2, and both of these designs produce almost the same maximum power density. However, considering the pressure drop over the flow field, the optimized design has a much lower pressure drop from the inlet to the outlet than the serpentine design. As seen in Fig. 7(c) and (e), and Table 6, the pressure drop is 270 Pa for the optimized design and 1011 Pa for the serpentine design. A lower pressure drop is better for the operation of PEM fuel cells and could reduce the need for an additional power supply, especially for a fuel cell with a large active area or a stack with a large number of fuel cell units. Fig. 7(a) shows that the pressure drop for the parallel design is only 226 Pa, which is even lower than the optimized design. This is because stagnant areas form in some channels of the parallel design, and the pressure drop in these channels is almost zero. For the optimized design, the pressure drop in every channel is required to be greater than zero in the optimization to satisfy the constraint that reactants flow through each channel at a certain flow rate. Combining the results from polarization curves and pressure distribution, the optimized design is

shown to have the advantages of both the serpentine design and the parallel design, performing as well as the serpentine design and having pressure drop as low as the parallel design. These merits of the optimized design result from the uniform distribution of pressure drops (Fig. 7 (e, f)) and the uniform transport of the reactant (Fig. 8 (c)).

The polarization curves in Fig. 6 from the multiple-serpentine design and the optimized design are compared further, according to the different regions of polarization curve. Note that there are three regions for a typical fuel cell polarization curve corresponding to three different kinds of losses, i.e., active losses, ohmic losses, and mass transport losses [15]. The active losses (the first portion of the polarization curve) are almost the same for these two designs because their operation conditions are the same. The two designs also show very similar ohmic losses. This can be seen from the middle portion of the polarization curve (i.e., the nearly linear portion). The ohmic losses are caused by the electrical (proton) resistances of the membrane, catalyst layer, GDL, and bipolar plates, and the contact resistances among them. All the resistances for the two designs are the same because the same materials are used, except the contact resistance between the GDL and the bipolar plates, which is mainly determined by the contact areas (land areas) between these two components and could be influenced by the design of flow field. In order to achieve fair comparison, in this study the flow fields are designed with the same land area, around 40% of the total flow field area. Therefore, the nearly same ohmic losses are obtained. Note that although 75% of the total flow field area is used as the channel surface area in the optimization model, the actual channel surface area is only 59.2% because there are lots of overlapping areas for channels sharing the same nodes. In the optimization model, these overlapping areas are not eliminated for the purpose of algorithmic simplification. From the last portion of the polarization curves, the optimized design can operate at as high as 3.0 A/cm^2 rather than 2.6 A/cm^2 for the multiple-serpentine design, before the voltage drops to 0.3 V. Therefore, the optimized design suffers much less mass transport losses than the serpentine design, indicating that the optimized design has much more efficient mass transport capabilities. Because of the better mass transport capability, the optimized design allows the fuel cell to work at a higher current density.

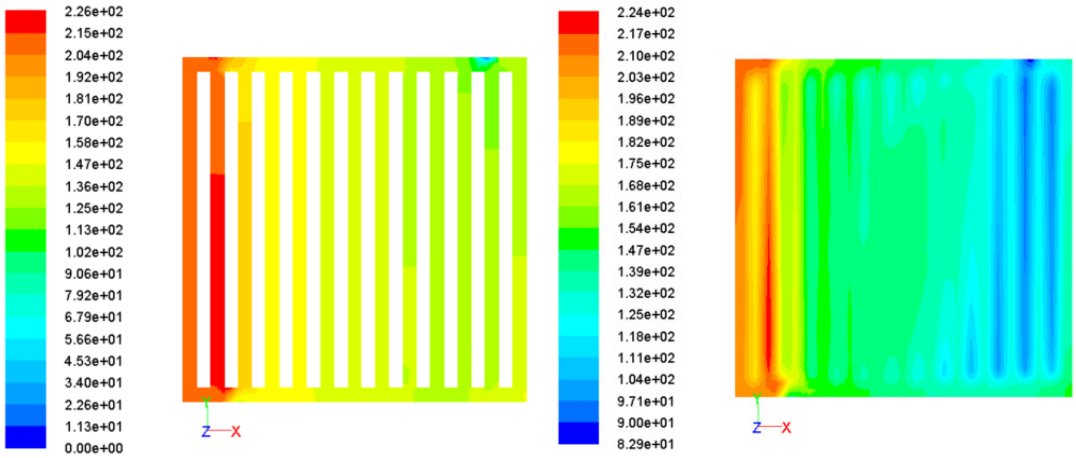

(a) (b)

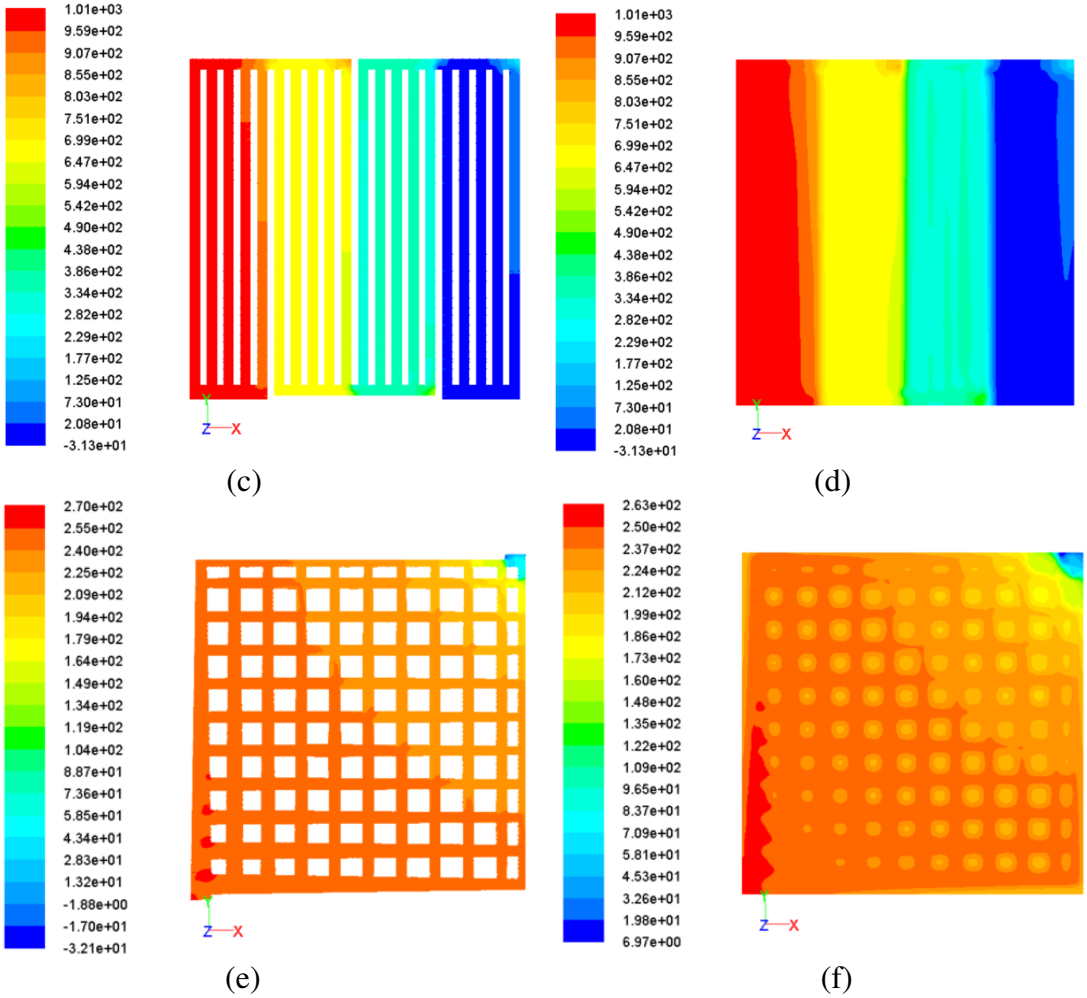

Fig. 7 Pressure (unit: Pa) distribution in the flow channels (a, c, e), and at the interface of the GDL and catalyst layer (b, d, f) on the cathode side at 0.55 V for (a, b) parallel design, (c, d) multiple-serpentine design, and (e, f) optimized design.

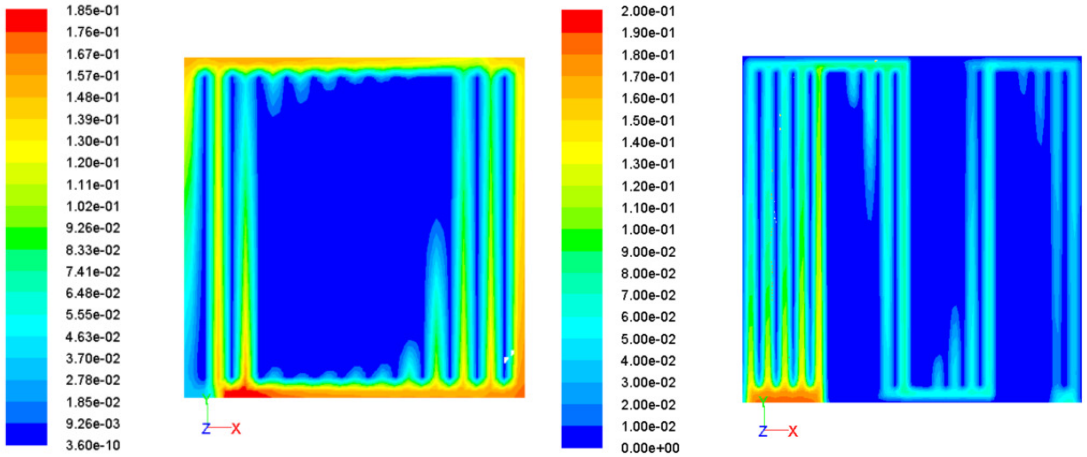

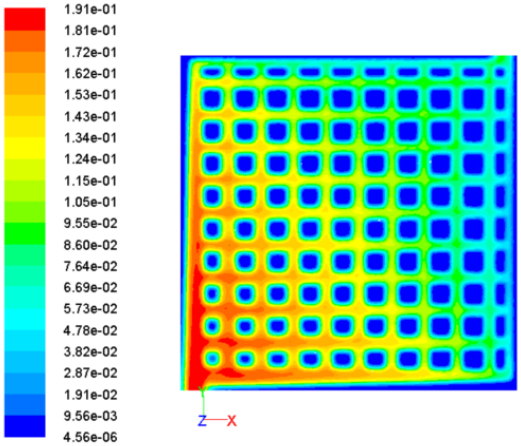

(c)

Fig. 8 Distribution of oxygen (volume fraction) at the interface of the GDL and catalyst layer on the cathode side at 0.55 V for (a) parallel design, (b) multiple-serpentine design, and (c) optimized design.

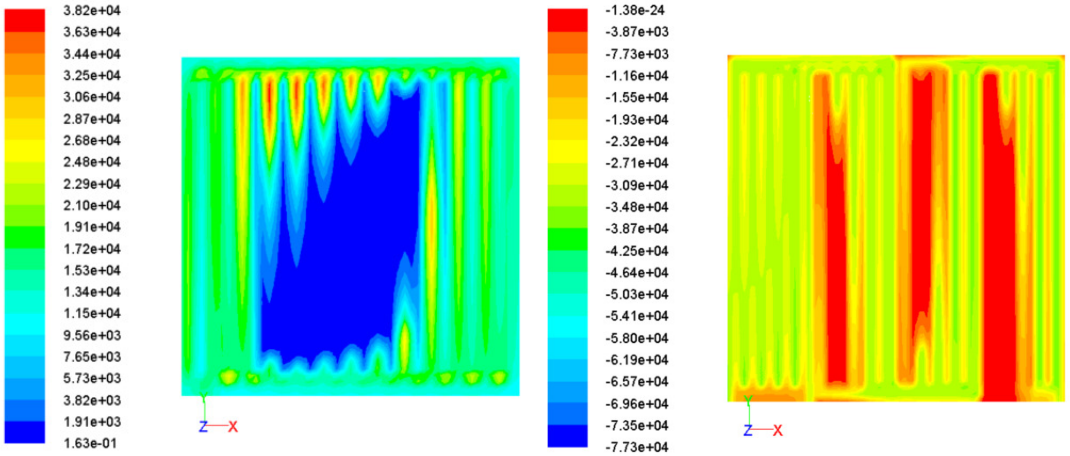

(a) (b)

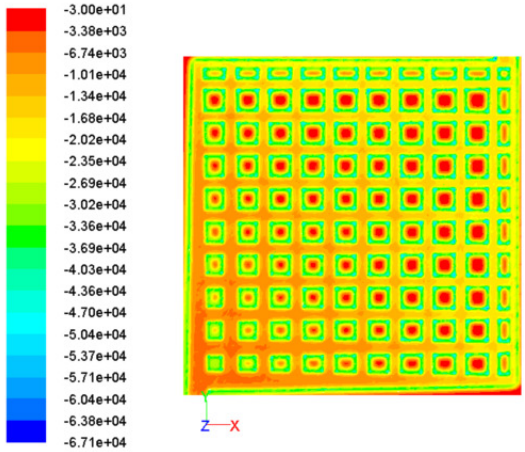

(c)

Fig. 9 Current density (unit: A/m^2) distribution at the interface of the GDL and catalyst layer on the cathode side at 0.55 V for (a) parallel design, (b) multiple-serpentine design, and (c) optimized design.

Comparing the pressure distribution of the three designs in Fig. 7, it is obvious that the optimized design has the most uniform pressure distribution over the whole flow field. Because the performance of a fuel cell is determined largely by the oxygen reduction reaction at the cathode, the distribution of oxygen is compared in Fig. 8. The catalyst surface of the optimized design has the largest area covered by oxygen, showing that it provides better mass transport of oxygen. The current density has a distribution (see Fig. 9) similar to oxygen because places receiving more oxygen generate more current. Note that the negative sign in the scale of Fig. 9 (b) and (c) indicates that the current is flowing in the reverse direction. Comparing these three designs in terms of performance, pressure distribution, oxygen distribution, and current density distribution leads to the conclusion that the optimized design provides power density as high as the serpentine design but with much lower pressure drop, more uniform pressure distribution, and more efficient mass transport capability. The optimized design also allows the fuel cell to work at a higher current density. Therefore, the proposed optimization model is suitable for the design of flow fields for bipolar plates and the improvement of PEM fuel cell performance.

5. Conclusions

An optimization model has been proposed for the design of flow fields in order to achieve a lower pressure drop in bipolar plates and higher PEM fuel cell performance. The optimization model generates flow field designs similar to structures found in nature (i.e., leaf veins). It also demonstrates this model's ability to optimize designs for any shapes of flow fields, any locations of inlets and outlets, and any desired flow properties. The comparison of FEM simulation results between the optimized design and the conventional parallel and multiple-serpentine designs has demonstrated that the optimized design can provide power density as high as the serpentine design but with much less pressure drop, more uniform pressure distribution, and more efficient mass transport capability. The optimized design also allows the fuel cell to work at a higher current density.

Acknowledgement

This project is supported by Air Force Research Laboratory under contract #FA8650-04-C-5704.

References

[1] Blunk, R., Elhamid, M. H., Lisi, D., Mikhail, Y. Polymeric composite bipolar plates for vehicle application. Journal of Power Sources, 2006, 156: 151-157.

[2] Watkins, D. S., Dircks, K. W., Epp, D. G. US Patent No. 5,108,849, 1992.

[3] Watkins, D. S., Dircks, K. W., Epp, D. G. US Patent No. 4,988,583, 1991.

[4] Li, X., Sabir, I. Review of bipolar plates in PEM fuel cells: Flow-field designs. International Journal of Hydrogen Energy, 2005, 30: 359-371.

[5] Li, X., Sabir, I., Park, J. A flow channel design procedure for PEM fuel cells with effective water removal. Journal of Power Sources, 2007, 163: 933-942.
[6] Misran, E., Daud, W. R. W., Majlan, E. H. Review on serpentine flow field design for PEM fuel cell system. Key Engineering Materials Vols, 2010, 447-448: 559-563.
[7] Kloess, J. P., Wang, X., Liu, J., Shi, Z., Guessous, L. Investigation of bio-inspired flow channel designs for bipolar plates in proton exchange membrane fuel cells. Journal of Power Sources, 2009, 188: 132-140.
[8] Chapman, A. and Mellor, I. Development of Biomimetic™ flow field plates for PEM fuel cells. The Eighth Grove Fuel Cell Symposium London, September 24–26, 2003.
[9] http://www.voltimum.co.uk/news/983/cm/fuel-cells-develop-further-with-uk-invention.html. Fuel cells develop further with UK invention. Morgan Fuel Cells (MFC).
[10] Damian-Ascencio, C., Hernandez-Guerrero, A., Ascencio-Cendejas, F. Entropy Generation Analysis for a PEM Fuel-Cell with a Biomimetic Flow Field. ASME 2009 International Mechanical Engineering Congress and Exposition. Florida, 2009.
[11] Wang, C. T., Hu, Y. C., Zheng, P. L. Novel biometric flow slab design for improvement of PEMFC performance. Applied Energy, 2010, 87: 1366-1375.
[12] Kjelstrup, S., Coppens, M. O., Pharoah, J. G., Pfeifer, P. Nature inspired energy and material efficient design of a polymer electrolyte membrane fuel cell. Energy & Fuels, 2010, 24: 5097-5108.
[13] Wang, X., Huang, Y., Cheng, C., Jang, J., Lee, D., Yan, W., Su, A. An inverse geometry design problem for optimization of single serpentine flow field of PEM fuel cell. International Journal of Hydrogen Energy, 2010, 35: 4247-4257.
[14] Peng, L., Lai, X., Yi, P., Mai, J., Ni, J. Design, optimization, and fabrication of slotted interdigitated thin metallic bipolar plates for PEM fuel cells. Journal of Fuel Cell Science and Technology, 2011, 8: 0110021-8.
[15] O'hayre, R. P., Cha, S. W., Colella, W. G., Prinz, F. B. Fuel cell fundamentals. 2nd ed. John Wiley & Sons, Inc., Hoboken, New Jersey, 2009, pp169-179.
[16] Tero, A., Takagi, S., Saigusa, T., Ito, K., Bebber, D. P., Fricker, M. D., Yumiki, K., Kobayashi, R., Nakagaki, T. Rules for Biologically Inspired Adaptive Network Design. Science, 2010, 327: 439-442.
[17] Banavar, J. R., Maritan, A., Rinaldo, A. Size and form in efficient transportation networks. Letters to nature, 1999, 399: 130-132.
[18] Katifori, E., Szollosi, G. J., Magnasco, M. O. Damage and Fluctuations Induce Loops in Optimal Transport Networks. Physical Review Letters, 2010, 104: 048704-4.
[19] Dodds, P. S. Optimal Form of Branching Supply and Collection Networks. Physical Review Letters, 2010, 104: 048702-4.
[20] Guo, N., Leu, M. C. Effect of Different Graphite Materials on Electrical Conductivity and Flexural Strength of Bipolar Plates Fabricated by Selective Laser Sintering. The 21th International SFF Symposium, Austin. Aug, 2010.
[21] Bourell, D. L., Leu, M. C., Chakravarthy, K., Guo, N., Alayavalli, K. Graphite-based indirect laser sintered fuel cell bipolar plates containing carbon fiber additions. CIRP Annals – Manufacturing Technology, 2011, 60: 275-278.
[22] Ferng, Y. M., Su, A. A three-dimensional full – cell CFD model used to investigate the effects of different flow channel designs on PEMFC performance. International Journal of Hydrogen Energy, 2007, 32: 4466-4476.

[23] Manso, A. P., Marzo, F. F., Garmendia Mujika, M., Barranco, J., Lorenzo, A. Numerical analysis of the influence of the channel cross-section aspect ratio on the performance of a PEM fuel cell with serpentine flow field design. International Journal of Hydrogen Energy, 2011, 36: 6795-6808.
[24] Iranzo, A., Munoz, M., Rosa, F., Pino, J. Numerical model for the performance prediction of a PEM fuel cell. Model results and experimental validation. International Journal of Hydrogen Energy, 2010, 35: 11533-11550.